Projectile K Auger spectra of Li-, Be-, and B-like multiply charged Ne ions: Auger energies, Auger rates, and intensity ratios

R. Bruch
Department of Physics, University of Nevada, Reno, Reno, Nevada 89557

D. Schneider and M. H. Chen
High Temperature Physics Division, Lawrence Livermore National Laboratory, P.O. Box 808, Livermore, California 94550

K. T. Chung and B. F. Davis*
Department of Physics, North Carolina State University, Raleigh, North Carolina 27650
(Received 28 March 1991)

In this work we have made an intense theoretical effort to determine accurate K-Auger transition energies, Auger rates, and line intensity ratios for Be- and B-like multiply charged neon ions using several different atomic models. Theoretical data on Li-like states in Ne VIII are also reported. In particular a detailed study of Auger line intensity ratios is presented. For several Be- and B-like states strong cancellations in the Auger matrix elements are predicted. These rates are quite sensitive to the atomic wave functions. We have also deduced experimental Auger intensity ratios for Be and B-like Ne ions from previous data. In order to classify our high-resolution projectile spectra, theoretical Auger energies and rates for various terms of the electron configurations $1s2s^22p^{n-1}$, $1s2p^{n+1}$, and $1s2s2p^n$ ($n=1-3$) have been calculated relativistically, using the saddle-point technique, the multiconfiguration Dirac-Fock model, and the $1/Z$ expansion method. Several previously unknown line identifications of Be-like states in Ne VII and B-like states in Ne VI are reported.

PACS number(s): 34.50.Fa, 31.20.Tz, 32.80.Hd

I. INTRODUCTION

Experimentally, isoelectronic separation and selective K-shell ionization or excitation has been accomplished by studying high-resolution, zero-degree [1–5] Ne Auger spectra induced by energetic $Ne^{q+}+He$ single collisions for various incident charge states. Such Ne K Auger spectra have been reported previously [6] however, the identification of several individual Be- and B-like Auger lines was hampered by the lack of reliable Auger transition energies and branching ratios. In this paper we present a more complete, revised line identification, in particular, for the Be- and B-like Auger lines on the grounds of theoretical Auger energies, Auger rates and line intensity ratios, calculated for a large number of core-excited states in Ne^{6+} and Ne^{5+}. For the first time we present here accurate experimental line intensity ratios for a select group of four- and five-electron systems that are in close agreement with our multiconfiguration Dirac-Fock (MCDF) predictions. Those intensity ratios provide important tests of electron correlation [7–17] and relativistic interactions [18–21] and have motivated a detailed comparison of Auger rates and intensity ratios for various existing theoretical models and different types of wave functions in Ne. To our knowledge, only very few recent KLL Auger rates exist in the literature for multiply charged Ne ions [22,23]. Thus, Ne K Auger transition probabilities for individual multiplets of Ne^{6+} ($1s2s^22p$), ($1s2s2p^2$) and Ne^{5+} ($1s2s^22p^2$) and ($1s2s2p^3$) configurations were calculated by Chen and Crasemann [23] and Bhalla [22] using the Hartree-Fock-Slater model. However, no configuration mixing was included in those computations.

Furthermore, Safronova and co-workers [17,24] studied Auger energies and rates along isoelectronic series by using many-body perturbation theory with $1/Z$ expansion. This approach predicts very strong and irregular Z dependencies for specific Auger rates affected by relativistic interactions of many levels of one inner-shell configuration [18]. As pointed out first by Kelly [8,9], Auger rates can sensitively depend on electron correlation and the details of the atomic wave function. In fact, Bruch *et al.* [2,3] have deduced ratios of partial Auger rates for the Be-like $(1s2s^22p)^3P^\circ$ and $^1P^\circ$ states in O V. For the $1s^22p:1s^22s$ intensity ratio, a value of about 16:1 has been reported which is caused by cancellation effects in the $(1s2s^22p)^1P^\circ \rightarrow (1s^22s\epsilon p)^1P^\circ$ channel. Such amplification of Auger intensity ratios due to cancellation effects may represent a new way of studying small changes of atomic many-body wave functions for highly excited states. We note that Bruch's experimental ratio for the $^1P^\circ$ state agrees with that of Nicolaides and Mercouris [12] who have analyzed the solution of the complex Schrödinger equation. Similar accidental cancellation effects for the $(1s2s^22p)^1P^\circ$ state were reported by Chen and Crasemann [23], Bhalla [22,25], Safronova and Vainshtein [18,24], Petrini [26], Mercouris and Nicolaides [13] for some ions of the Be-isoelectronic series. Recently Caldwell *et al.* [27] have measured a near 100% production of Be II ($1s^22p$) ions following Auger decay of the $(1s2s^22p)^1P^\circ$ state in neutral beryllium.

Such "symmetry preferred" Auger transitions [28] populating selectively specific excited bound states are not only important to test the details of atomic few-body theories of multiply charged ions, but may also play a fundamental role for the conceptional design of extreme ultraviolet (EUV) lasers [29–31] and the understanding of laser-induced plasmas [32,33]. These final-state selective Auger cascades arising from multiply ionized highly excited states may also be important in connection with astrophysics, surface science, absolute cross-section measurements following ion-atom collisions, and are relevant for selective inner-shell photoexcitation or ionization processes using future intense soft x-ray light sources such as the advanced light source (ALS) [34].

This paper is organized as follows. In Sec. II, two different variational procedures, i.e., the saddle-point technique [35–38] that includes relativistic corrections and the multiconfiguration Dirac-Fock model [7] have been applied to predict Auger energies, Auger rates, and intensity ratios for Li-, Be-, and B-like states of Ne. One of the main goals of these calculations has been to provide information on exceptionally large, "amplified" Auger intensity ratios owing to cancellation effects in Auger transition probabilities caused by electron correlation, and relativistic corrections. In Sec. III a detailed comparison for all predicted Auger energies, Auger rates, and intensity ratios is provided for various models and approximations.

The experimental procedure for measuring high-resolution zero-degree projectile K Auger spectra [1–6] is briefly outlined in Sec. IV. In this section we also present characteristic high-resolution Ne K Auger sample electron spectra associated with Li-, Be-, and B-like multiply charged neon states. The corresponding line assignment for these projectile spectra is given in Sec. V. In addition, in Sec. VI we present Auger line intensity ratios originating from four- and five-electron systems in Ne. Finally, Sec. VII summarizes our experimental and theoretical results.

II. CALCULATED AUGER ENERGIES AND RATES

A. Saddle-point technique

Using a saddle-point method [35–38], the Li-like $1s2l2l'$ states and the Be-like $(1s2s^2 2p)^3P^\circ$ resonance are calculated for the nuclear charge $Z=10$. The saddle-point method for four-electron systems parallels that for three-electron systems [37]. The nonrelativistic part of the calculation closely follows the procedure developed by Chung [35]. The relativistic correlations given in this study are calculated within the framework of the Breit-Pauli approximation, using first-order perturbation theory [38]. In computing the energy of the $(1s2s^2 2p)^3P^\circ$ state in Ne VII, we have found that both radial and angular correlations strongly affect the calculated Auger energy position. In order to achieve high accuracy for the resonance energy of the $(1s2s^2 2p)^3P^\circ$ state, we have incorporated 260 terms and 29 various orbital and spin angular coupling partial waves in the wave function of the $Ne^{7+}+e^-$ scattering problem. Our *ab initio* results predicted by the saddle-point method are presented in Tables I and II. Relativistic corrections include the mass correction, Darwin term, electron-electron contact term, and orbit-orbit interaction (retardation potential). The mass polarization effect is also included in this correction. As can be seen from Table I, the lowest, singly, core-excited resonance in Ne VIII is $(1s2s^2)^2S$. Among the doublets formed by the $(1s2s2p)$ configuration, the $[1s(2s2p)^3P]^2P^\circ$ is the lowest followed by $[1s(2s2p)^1P]^2P^\circ$. Other results given in Table I are the $(1s2p^2)^2D$, ^2S, and $[(1s2s)^3S3d]^2D$ Coulomb autoioniz-

TABLE I. K-shell Auger energies for lithium-like states originating from $1s2s^2$, $1s2s2p$, $1s2p^2$, and $1s2s3d$ configurations in Ne VIII. The nonrelativistic energies have been computed by means of the saddle-point method. Relativistic effects due to the mass kinetic-energy (KE) correction, Darwin term, electron-electron contact term, and orbit-orbit interaction have been taken into account. The mass polarization effect is also accounted for. E_{Nonrel} is the nonrelativistic energy, E_{Tot} is the relativistic energy, and E_{Auger} is the energy of the Auger electron computed using the relativistic-with-Lamb-shift ground-state energy for Ne IX $(1s^2)^1S$ 94.013 644 a.u. of Pekeris *et al.* [Phys. Rev. **112**, 1649 (1958)]. (All energy values given in a.u. except E_{Auger}. 1 a.u. of energy = 27.210 859 0 eV.)

Resonance	E_{nonrelat}	L	N	$10^1\langle H1+H2\rangle$ rel. KE +Darwin	$10^3\langle H3\rangle$ Fermi contact	$10^4\langle H4\rangle$ orbit-orbit	$10^4\langle H5\rangle$ mass polariz.	E_{tot}	E_{Auger} (eV)
$(1s2s2s)^2S$	−69.933 812	14	97	−0.940 799	+0.4878	+0.491	−0.125	−70.028 368	652.66
$(1s2s2p)^4P^\circ$	−69.780 524	12	80	−0.882 639	0	+10.095	−1.590	−69.867 937	657.03
$[1s(2s2p)^3P]^2P^\circ$	−69.337 290	16	106	−0.865 488	+0.7728	−6.7615	+1.278	−69.423 615	669.12
$(1s2p2p)^4P$	−69.163 729	11	78	−0.781 312	0	+20.395	−3.143	−69.240 135	674.11
$[1s(2s2p)^1P]^2P^\circ$	−69.121 472	16	108	−0.862 800	+0.4992	+7.1384	−1.266	−69.206 665	675.02
$(1s2p2p)^2D$	−68.894 912	14	103	−0.780 628	+0.2068	+7.999	−1.589	−68.972 127	681.40
$(1s2p2p)^2P$	−68.803 531	15	89	−0.777 961	+0.3723	−7.073	+1.586	−68.881 668	683.86
$(1s2p2p)^2S$	−68.473 569	13	104	−0.793 585	+0.3846	+11.226	−1.242	−68.551 545	692.85
$[(1s2s)^3S3d]^2D$	−64.271 140	13	74	−0.836 191	+0.0371	+0.2596	−0.060	−64.354 703	807.05

TABLE II. Our values for the resonance energy E of the $(1s2s^22p)^3P^\circ$ state of Be-like Ne VII obtained from the saddle-point method. E_{nonrel} is the nonrelativistic energy and E the relativistic energy. The relativistic corrections ΔE_{rel} include the mass correction, Darwin term, electron-electron contact term, and orbit-orbit term (retardation potential). The mass polarization effect is also included in this correction. The relativistic bound-state $(1s^22p)^2P^\circ$ energy has been determined by a configuration interaction wave function. [Decay channel energy of the $(1s^22p)^2P^\circ$ state in Ne^{7+}: $-102.213\,177$ a.u. this work. Fine-structure splitting $\Delta E(\frac{1}{2},\frac{3}{2})$ of the $(1s^22p)^2P^\circ$ state in Ne^{7+}: 0.204 eV, this work.]

E_{nonrel}	ΔE_{rel} relativistic correction	$E=E_{\text{nonrel}}+\Delta E_{\text{rel}}$
$-77.595\,426$	$-0.096\,956$	$-77.692\,382$

ing states, as well as the $(1s2s2p)^4P$, $(1s2p^2)^4P$, and ^2P terms, which are metastable with respect to Coulomb autoionization. The energies of these metastable autoionizing levels have been calculated using an LSJ coupling scheme and configuration interaction wave functions. The Ne VIII $(1s2s2p)^4P^\circ$ state is of particular importance because it can be used to accurately calibrate experimental Ne K Auger spectra (see Sec. V). We further note that the lowest, singly, core-excited state in Ne^{6+}, namely, $(1s2s^22p)^3P^\circ$, is of great theoretical interest, since it represents a K-vacancy state with two competing decay channels, i.e., $(1s^22s\epsilon p)^2P^\circ$ and $(1s^22p\epsilon s$ or $\epsilon d)^2P^\circ$ (see also Secs. III and VI). In addition to the $(1s2s^22p)^3P^\circ$ excitation energy for Ne VII, we have also calculated the relativistic Ne VIII $(1s^22p)^2P^\circ$ channel energy and the corresponding $^2P^\circ(\frac{1}{2},\frac{3}{2})$ fine-structure splitting (see Table II). We note that the obtained $J=\frac{1}{2}$-$J=\frac{3}{2}$ level separation of 0.204 eV cannot be resolved in our experiment (see Sec. IV).

B. Multiconfigurational Dirac-Fock calculations

The Auger energies and transition probabilties are calculated in perturbation theory with the frozen orbital approximation [39]. In the multiconfiguration Dirac-Fock model [40], an atomic state function for a state i with total angular momentum JM is expanded in terms of n configuration state functions (CSF) [41]:

$$\psi_i(JM)=\sum_{\lambda=1}^{n} C_{i\lambda}\phi(\Gamma_\lambda JM)\ , \tag{1}$$

where $C_{i\lambda}$ are the mixing coefficients for state i. The total Auger transition rate from the initial ionic state i to the final ionic state f, based on the MCDF model, is given by [41]

$$T_{\text{fi}}=2\pi\sum_{j_c}\left|\sum_{\lambda}\sum_{\lambda'} C_{i\lambda}C_{f\lambda'}A_{\lambda\lambda'}\right|^2\ , \tag{2}$$

where

$$A_{\lambda\lambda'}=\left\langle\phi(\Gamma_{\lambda'}J'M'\epsilon j_c;JM)\left|\sum_{\alpha(<\beta)} V_{\alpha\beta}\right|\phi(\Gamma_\lambda JM)\right\rangle\ . \tag{3}$$

Here, the continuum wave function ϵj_c is normalized in energy.

TABLE III. Calculated K-shell Auger energies and rates for the $1s2s^22p$ and $1s2s2p^2$ configurations of Be-like Ne VII. Orbital wave functions and atomic energy levels have been calculated in the MCDF model. The relativistic Auger transition rates are computed by perturbation theory in the MCDF approximation. (Numbers in square brackets indicate powers of 10, e.g., 9.58[13] means 9.58×10^{13}.)

Auger transition		Auger energy (eV)	Auger rate (sec^{-1})
$1s2s^22p$	$^3P^\circ\rightarrow(1s^22p)^2P^\circ$	667.83	9.58[13]
	$^3P^\circ\rightarrow(1s^22s)^2S$	683.97	5.04[13]
	$^1P^\circ\rightarrow(1s^22p)^2P^\circ$	674.17	9.76[13]
	$^1P^\circ\rightarrow(1s^22s)^2S$	690.31	4.09[11]
$1s2s2p^2$	$^5P\rightarrow(1s^22p)^2P^\circ$	670.13	8.26[8]
	$^3_bP\rightarrow(1s^22p)^2P^\circ$	684.57	3.14[13]
	$^3D\rightarrow(1s^22p)^2P^\circ$	685.28	1.03[13]
	$^3S\rightarrow(1s^22p)^2P^\circ$	692.34	1.03[13]
	$^1D\rightarrow(1s^22p)^2P^\circ$	694.71	1.29[14]
	$^3_aP\rightarrow(1s^22p)^2P^\circ$	696.48	1.18[14]
	$^1S\rightarrow(1s^22p)^2P^\circ$	701.83	1.21[14]
	$^1P\rightarrow(1s^22p)^2P^\circ$	701.42	3.13[13]
	$^5P\rightarrow(1s^22s)^2S$	686.31	3.87[9]
	$^3_bP\rightarrow(1s^22s)^2S$	700.71	9.47[11]
	$^3D\rightarrow(1s^22s)^2S$	701.42	1.04[14]
	$^3S\rightarrow(1s^22s)^2S$	708.47	4.62[13]
	$^1D\rightarrow(1s^22s)^2S$	710.84	1.11[14]
	$^3_aP\rightarrow(1s^22s)^2S$	712.62	1.58[11]
	$^1S\rightarrow(1s^22s)^2S$	717.96	5.06[13]
	$^1P\rightarrow(1s^22s)^2S$	717.56	1.44[9]

The two-electron operator $V_{\alpha\beta}$ is taken to be the sum of the Coulomb and generalized Breit operator [41,42]:

$$V_{12}=\frac{1}{r_{12}}-(\boldsymbol{\alpha}_1\cdot\boldsymbol{\alpha}_2)\frac{\cos(\omega r_{12})}{r_{12}}+(\boldsymbol{\alpha}_1\cdot\boldsymbol{\nabla}_1)(\boldsymbol{\alpha}\cdot\boldsymbol{\nabla}_2)\frac{\cos(\omega r_{12})-1}{\omega^2 r_{12}}\ , \tag{4}$$

where the α_i are the Dirac matrices and ω is the wave number of the exchanged virtual photon. In Eqs. (2)–(4), atomic units are used.

The energies and wave functions for initial and final states were calculated separately using the MCDF model with an average-level scheme [40]. The Auger radial matrix elements were evaluated by using the orbital wave functions from the initial state. The continuum wave functions were generated by solving the Dirac-Fock equations corresponding to the final state without the exchange interaction between the bound and continuum electrons. A Schmidt orthogonalization to the initial orbital wave functions is then performed. The angular factors of the Auger matrix elements $A_{\lambda\lambda'}$ were obtained by using slightly modified general angular momentum subroutines [40,44].

Tables III and IV summarize our MCDF results for Auger transition energies and rates. Specifically, in Table III, Ne K Auger energies and multiplet partial Auger rates are presented for the Be-like $1s2s^22p$ and $1s2s2p^2$ configurations and the corresponding data for B-like $1s2s^22p^2$ and $1s2s2p^3$ configurations are listed in Table IV. The Auger rates are expressed in the unites $\sec^{-1}$. It is evident that the calculated multiplet partial Auger rates vary significantly for the various transitions. For example, the predominant decay mode for the Ne VII $(1s2s^22p)^1P^\circ$ state is Ne VIII $(1s^22p)$, rather than Ne VIII $(1s^22s)$. Thus, the predicted MCDF $(1s^22p\epsilon s$ or $\epsilon d)$ branching ratio is about 99.58% when compared to a ratio of 0.42% for the $(1s^22s\epsilon p)$ Auger decay channel. Such dramatic differences in Auger line intensities are, of course, of great significance for the identification of experimental Ne K Auger electron spectra. A more detailed discussion of the obtained rates and Auger intensity ratios is presented in Secs. III and VI.

TABLE IV. Calculated K-shell Auger energies and rates for the $1s2s^22p^2$ and $1s2s2p^3$ configurations of B-like Ne VI. Orbital wave functions and atomic energy levels have been calculated in the MCDF model. The relativistic Auger transition rates are computed by perturbation theory in the MCDF approximation. (Again, powers of 10 appear in square brackets.)

Auger transition		Auger energy (eV)	Auger rate ($\sec^{-1}$)
$1s2s^22p^2(^3P)$	$^4P\rightarrow(1s^22s^2)^1S$	719.11	1.79[10]
	$^4P\rightarrow(1s^22s2p)^3P^\circ$	705.06	9.15[13]
	$^4P\rightarrow(1s^22s2p)^1P^\circ$	690.81	3.31[9]
	$^4P\rightarrow(1s^22p^2)^1S$	668.46	7.50[8]
	$^4P\rightarrow(1s^22p^2)^3P$	682.79	7.49[13]
	$^4P\rightarrow(1s^22p^2)^1D$	678.35	2.83[9]
$1s2s^22p^2(^3P)$	$^2P\rightarrow(1s^22s^2)^1S$	727.51	4.88[11]
	$^2P\rightarrow(1s^22s2p)^3P^\circ$	713.46	2.91[12]
	$^2P\rightarrow(1s^22s2p)^1P^\circ$	699.21	2.16[13]
	$^2P\rightarrow(1s^22p^2)^1S$	676.87	4.96[10]
	$^2P\rightarrow(1s^22p^2)^3P$	691.19	7.39[13]
	$^2P\rightarrow(1s^22p^2)^1D$	686.75	6.11[11]
$1s2s2p^3$	$^6S\rightarrow(1s^22s^2)^1S$	719.74	0.0
	$^6S\rightarrow(1s^22s2p)^3P^\circ$	705.68	7.62[9]
	$^6S\rightarrow(1s^22s2p)^1P^\circ$	691.43	1.47[4]
	$^6S\rightarrow(1s^22p^2)^1S$	669.09	0.0
	$^6S\rightarrow(1s^22p^2)^3P$	683.42	5.61[8]
	$^6S\rightarrow(1s^22p^2)^1D$	678.98	4.89[6]
$1s2s(^3S)2p^3$	$^4S\rightarrow(1s^22s^2)^1S$	735.75	6.72[7]
	$^4S\rightarrow(1s^22s2p)^3P^\circ$	721.69	6.78[10]
	$^4S\rightarrow(1s^22s2p)^1P^\circ$	707.44	1.47[8]
	$^4S\rightarrow(1s^22p^2)^1S$	685.10	7.92[6]
	$^4S\rightarrow(1s^22p^2)^3P$	699.43	3.91[13]
	$^4S\rightarrow(1s^22p^2)^1D$	694.99	3.94[9]
$1s2s(^1S)2p^3$	$^4S\rightarrow(1s^22s^2)^1S$	752.52	5.14[8]
	$^4S\rightarrow(1s^22s2p)^3P^\circ$	738.47	4.73[10]
	$^4S\rightarrow(1s^22s2p)^1P^\circ$	724.22	7.17[10]
	$^4S\rightarrow(1s^22p^2)^1S$	701.88	2.71[8]
	$^4S\rightarrow(1s^22p^2)^3P$	716.21	1.56[14]
	$^4S\rightarrow(2s^22p^2)^1D$	711.77	1.47[10]

C. $1/Z$ expansion method

Ne *K* Auger positions and Auger rates as well as intensity ratios of some of the main excited terms of Ne^{5+}, Ne^{6+}, and Ne^{7+} have also been determined in this work using the $1/Z$ expansion method [17,18]. Relativistic effects have been included in the Breit-operator form. This many-body perturbation method has been developed by Ivanova and Safronova [18]. Since the electron energy resolution in projectile Auger spectra is not sufficient to resolve individual fine-structure components, effective Auger rates of a given ^{2S+1}L term have been deduced from unpublished predictions of Safronova [24] and Dubau [24]. Assuming statistical population of the different levels, we define the average Auger rate for a specific term as

$$\overline{A}(LS)=\frac{\sum_J (2J+1)A(LSJ)}{\sum_J (2J+1)}\ , \tag{5}$$

where the $A(LSJ)$ are the J-dependent Auger transition probabilities and the summation extends over all possible J quantum numbers that belong to the given ^{2S+1}L state. The deduced $1/Z$ Auger energies and rates for the various Ne^{6+} terms of electron configurations $1s2s^2 2p$ and $1s2s2p^2$ are listed in Table V along with other theoretical predictions.

In addition, $1/Z$ Auger line intensity ratios for all Ne VII terms pertaining to the configurations $1s2s^2 2p$ and $1s2s2p^2$ are given in Table VI. Some of the striking features of these four-electron Auger rates and intensity ratios are discussed in the following section.

TABLE V. Comparison of relativistically calculated *K* Auger transition energies and rates for all terms originating from the $1s2s^2 2p$ and $1s2s2p^2$ initial configurations of Be-like Ne VII for different theoretical models. For example, $1.57[14]=1.57\times10^{14}$ sec^{-1}. As in Tables III and IV, powers of 10 appear in square brackets.

	Auger transition energies (eV)			Auger rates (sec^{-1})					
Auger transition	Saddle-point method[a]	$1/Z$[b]	MCDF[c]	$1/Z$[b]	MCDF[c]	SUPERSTRUCTURE AUTO *LSJ*[d]	$(Z\text{-}3)$[e]	HFS[f]	HFS[g]
$(1s2s^2 2p)^3P^\circ \rightarrow (1s^2 2p)^2P^\circ$	667.27	666.95	667.83	7.04[13]	9.58[13]	10.06[13]	8.45[13]	6.36[13]	6.51[13]
$^3P^\circ \rightarrow (1s^2 2s)^2S$	683.295	682.97	683.97	7.56[13]	5.04[13]	4.84[13]	5.00[13]	4.74[13]	4.90[13]
$(1s2s^2 2p)^1P^\circ \rightarrow (1s^2 2p)^2P^\circ$		673.26	674.17	7.445[13]	9.76[13]	10.05[13]	8.445[13]	6.36[13]	6.51[13]
$^1P^\circ \rightarrow (1s^2 2s)^2S$		689.29	690.31	2.35[12]	4.09[11]	3.54[11]	5.59[11]	1.15[11]	2.27[11]
$(1s2s2p^2)^5P \rightarrow (1s^2 2p)^2P$		670.50	670.13	1.6[9]	8.26[8]	8.1[8]	9.00[8]	8.04[8]	
$^5P \rightarrow (1s^2 2s)^2S$		686.53	686.31	1.0[10]	3.87[9]	5.7[9]	1.0[10]	4.75[9]	
$[1s2s(^3S)2p^2]^3_aP \rightarrow (1s^2 2p)^2P^\circ$		684.28	684.57	8.69[13]	3.14[13]	1.61[13]	2.79[13]	1.78[13]	
$^3_aP \rightarrow (1s^2 2s)^2S$		700.31	700.71	3.44[13]	9.47[11]	3.2[12]	4.14[11]		
$[1s2s(^3S)2p^2]^3D \rightarrow (1s^2 2p)^2P^\circ$		683.99	685.28	3.08[13]	1.03[13]	1.50[13]	1.00[13]	1.35[13]	
$^3D \rightarrow (1s^2 2s)^2S$		700.24	701.42	1.66[14]	1.04[14]	1.07[14]	1.16[14]	9.95[13]	
$[1s2s(^3S)2p^2]^3S \rightarrow (1s^2 2p)^2P^\circ$		691.575	692.34	3.03[13]	1.03[13]	1.50[13]	1.11[13]	1.35[13]	
$^3S \rightarrow (1s2s)^2S$		707.60	708.47	7.77[13]	4.62[13]	4.14[13]	5.74[13]	3.99[13]	
$[1s2s(^3S)2p^2]^1D \rightarrow (1s^2 2p)^2P^\circ$		693.18	694.71	1.55[14]	1.29[14]	1.12[14]	1.31[14]	1.03[14]	
$^1D \rightarrow (1s^2 2s)^2S$		709.21	710.84	1.86[14]	1.11[14]	1.08[14]	1.10[14]	9.95[13]	
$[1s2s(^1S)2p^2]^3_bP \rightarrow (1s^2 2p)^2P^\circ$			696.48	1.57[14]	1.18[14]	1.26[14]	1.26[14]	1.13[14]	
$^3_bP \rightarrow (1s^2 2s)^2S$			712.62	3.11[11]	1.58[11]	2.04[11]	4.53[11]	0	
$[1s2s(^1S)2p^2]^1S \rightarrow (1s^2 2p)^2P^\circ$		700.54	701.83	1.60[14]	1.21[14]	1.12[14]	1.31[14]	1.03[14]	
$^1S \rightarrow (1s^2 2s)^2S$		716.57	717.96	7.78[13]	5.06[13]	4.14[13]	5.77[13]	3.99[13]	
$[1s2s(^1S)2p^2]^1P \rightarrow (1s^2 2p)^2P^\circ$			701.42	8.31[13]	3.13[13]	4.45[13]	3.10[13]	4.05[13]	
$^1P \rightarrow (1s^2 2s)^2S$			717.56	1.62[10]	1.44[9]	8.2[10]	1.72[10]	0	

[a]Saddle-point method including relativistic corrections by means of the Breit-Pauli approximation, this work.

[b]$1/Z$ method (Refs. [17,24]) and this work.

[c]Multiconfiguration Dirac-Fock model, this work.

[d]SUPERSTRUCTURE PLUS AUTOIONIZATION *LSJ* COUPLING (Refs. [45,46]).

[e]$Z_s=Z$-3 model (Ref. [24]).

[f]Hartree-Fock-Slater model (Ref. [23]).

[g]Hartree-Fock-Slater model (Ref. [22]).

TABLE VI. Comparison of theoretically predicted $1s^2 2p$:$1s^2 2s$ Auger line intensity ratios for the different terms arising from the $1s2s^2 2p$ and $1s2s2p^2$ initial configurations of Be-like Ne VII.

Initial state	$1/Z$[a]	MCDF[b]	SUPERSTRUCTURE[c] AUTO (LSJ)	$Z_s=(Z\text{-}3)$[d]	HFS[e]	HFS[f]
$(1s2s^2 2p)^3P^\circ$	0.93	1.90	2.08	1.69	1.34	1.33
$(1s2s^2 2p)^1P^\circ$	31.7	238.6	283.9	151.1	553	286.8
$(1s2s2p^2)^5P$	0.16	0.21	0.14	0.09	0.17	
$(1s2s2p^2)^3_aP$		331.6	5.0	673.9		
$(1s2s2p^2)^3D$	0.19	0.10	0.14	0.09	0.14	
$(1s2s2p^2)^3S$	0.39	0.22	0.36	0.19	0.34	
$(1s2s2p^2)^1D$	0.83	1.16	1.04	1.19	1.04	
$(1s2s2p^2)^3_bP$	504.8	746.8	617.6	278.1		
$(1s2s2p^2)^1S$	2.06	2.39	2.71	2.27	2.58	
$(1s2s2p^2)^1P$	5130	2140	542.7	1800		

[a] $1/Z$ method (Refs. [17] and [24]) and this work.
[b] Multiconfiguration Dirac-Fock model, this work.
[c] Superstructure plus autoionization program codes, *LSJ* coupling, Dubau (Ref. [24]).
[d] $Z_s=(Z\text{-}3)$ screening model (Ref. [24]).
[e] Hartree-Fock-Slater model (Ref. [23]).
[f] Hartree-Fock-Slater model (Ref. [22]).

III. COMPARISON OF Be-LIKE AUGER ENERGIES AND RATES FOR DIFFERENT ATOMIC MODELS

A systematic comparison of calculated Auger transition energies and rates for Be-like Ne^{6+} ions has been performed as a function of different atomic models. The results of all calculated Auger line positions and rates are summarized in Table V for the $1s2s^2 2p$ and $1s2s2p^2$ initial configurations in Ne VII.

It is interesting to compare first the Auger energies. Although the MCDF model and the Superstructure code, as well as the $1/Z$ expansion method, include configuration mixing to some extent, the saddle-point method incorporates the most complete description of electron-electron interactions [37] and hence provides the most accurate energy predictions. Since the Breit interaction is already quite important for highly excited neon ions, all Ne K Auger energies given in Table V have been corrected for relativistic energy shifts [14,17]. We note that, for the Be-like states listed in Table V, the possible and final states after Auger decay are $(1s^2 2p)^2P^\circ$ and $(1s^2 2s)^2S$. For the studied $1s2s^2 2p$ and $1s2s2p^2$ configurations, LS notation is used leading to ten different Auger states, namely, $(1s2s^2 2p)^3P^\circ$ and $^1P^\circ$ $(1s2s2p^2)^3D$, ^1D, ^5P, ^3_aP, ^3_bP, ^1P, ^3S, and ^1S.

Electron correlation directly affects Auger line energies. The most accurate numerical result of this paper is the

$$(1s2s^2 2p)^3P^\circ \rightarrow (1s^2 2p\epsilon s \text{ or } \epsilon d)^3P^\circ$$

transition energy of 667.27 eV derived from the saddle-point method. This value has to be compared with the $1/Z$ expansion and MCDF results of 666.95 and 667.83 eV, respectively. As can be seen, the MCDF energy is 0.56 eV higher and the $1/Z$ expansion prediction 0.32 eV lower than the variationally obtained energy by the saddle-point technique. We therefore conclude that the $1/Z$ and MCDF Auger transition energies are accurate to within a few tenths of an eV.

The $1/Z$ expansion method and the MCDF model have been further applied in obtaining Auger rates and line-intensity ratios which are listed in Tables V and VI along with predictions using the SUPERSTRUCTURE AUTO *LSJ* code (SUPERSTRUCTURE PLUS AUTOIONIZATION *LSJ* COUPLING code [45,46]) and the Z-3 screening model [24]. In the Z-3 method, the radial integrals were evaluated with hydrogenic orbitals, but for continuous states, Coulomb wave functions with effective charge $Z-3$ were used. For completeness we have also tabulated the Hartree-Fock-Slater results of Chen and Crasemann [23] and Bhalla [22].

The MCDF Auger rates presented in Table V have been computed in intermediate coupling, including configuration interaction within the $1s2l'^m 2l''^n$ $(m+n=3)$ complex. Nevertheless, we have designated all Be-like states in Ne VII according to the dominant *LSJ* eigenvector component. It is apparent from Table V that the radial matrix elements evaluated with the MCDF model give slightly larger rates than those based on the Thomas-Fermi model (SUPERSTRUCTURE AUTO *LSJ* [44,45]). It is also evident from Table V that the rates obtained from hydrogenic orbitals and Coulomb wave functions (Z-3 model) deviate from those based on the MCDF method. We have also discovered that inclusion of electron-electron correlation corrections has a pronounced effect on Auger rates. In particular, weak transitions, which involve large cancellation effects in Auger matrix elements, are sensitive to differences in atomic wave functions. A strong wave-function dependence is found, for example, for the

$$(1s2s^2 2p)^1P^\circ \rightarrow (1s^2 2s\epsilon p)^1P^\circ$$

transition. Thus, by using the Hartree-Fock-Slater model, a rate of 1.15×10^{11} sec^{-1} is predicted, whereas with the MCDF model we obtain a value of 4.09×10^{11} sec^{-1}, which is about four times larger.

Finally, we note that the $1/Z$-expansion method predicts rates which strongly deviate in most cases from the corresponding MCDF and SUPERSTRUCTURE AUTO LSJ data. In this paper we have also undertaken a systematic study of line intensity ratios (see Table VI). In particular, we are interested here in very large Auger ratios which "amplify" the effects of electron correlations and relativistic mixings. We have found evidence in this study that this phenomenon does not only exist for the $(1s2s^22p)^1P^\circ$ states, but plays also a fundamental role for the Auger decay of the Be-like $(1s2s2p^2)^3_aP$, ^3_bP, and ^1P states. Specifically, the $(1s2s2p^2)^1P$ state in Ne VII is forbidden to decay to the $1s^22s$ state by Coulomb interaction. This leads to a dramatic amplification of the $1s^22p$:$1s^22s$ ratio of the order of 2140:1 (MCDF model). The strong variation of this ratio between 542.7:1 and 5130:1 clearly indicates that this amplification effect is strongly model dependent. Similar anomalies in Auger intensities occur for B-like single K-vacancy states of Ne VI as indicated in Table IV. We have also provided evidence in this study that the $[1s2s^22p^2(^3P)]^4P$ and ^2P states are characterized by two dominant Auger channels only, whereas the $[1s2s(^3S)2p^3]^6S^\circ$, $^4S^\circ$, and $[1s2s(^1S)2p^3]^4S^\circ$ terms decay predominantly through one single channel (see Table IV). In this context we would like to emphasize that those extremely weak Auger transitions predicted in this work are difficult to observe via projectile Auger spectroscopy but could be revealed in greater clarity in the near future by using intense monochromatic x-ray radiation, as provided by the advanced light source [34].

IV. EXPERIMENTAL PROCEDURE

High-resolution zero-degree measurements of Ne K Auger electron spectra using multiply charged Ne projectile ions in collisions with He, H_2, and Ar at impact energies of 70 and 100 MeV have been reported previously [6]. The experimental setup is similar to the one used in Refs. [1–6]. In brief, a tightly collimated beam of energetic Ne^{6+}, Ne^{5+}, or Ne^{4+} ions has been accelerated at the Hahn-Meitner Institut für Kernforschung (HMI) Berlin heavy-ion accelerator facility VICKSI and focused onto a gas cell of 4 cm length. The gas pressure in the target area has been kept constant at about 10 mTorr to ensure single-collision conditions. Following inner-shell ionization, the projectile beam then transverses the first stage of an electrostatic 45° parallel-plate analyzer of a tandem electron spectrometer [3,4]. For normalization purposes, the beam current has been measured in a Faraday cup. The deflected zero-degree projectile Auger electrons have been analyzed by means of the second-stage high-resolution electron spectrometer. With this arrangement Li-, Be-, and B-like electron configurations have been selectively produced for Ne^{6+}, Ne^{5+}, and Ne^{4+} ions colliding with He. Characteristic samples of the corresponding Auger electron spectra are displayed in Figs. 1–3.

The majority of the projectile Auger lines as indicated in Figs. 1–3 and Tables VII–IX originate from three-, four-, and five-electron neon ions, in accordance with the selective K-shell ionization phenomenon in the case of fast multiply charged ions incident on light target atoms [6] such as He. However, K-shell ionization plus simul-

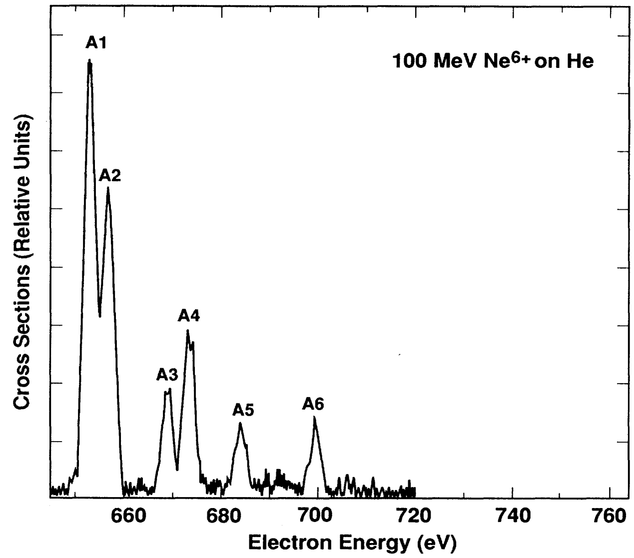

FIG. 1. High-resolution zero-degree electron spectrum produced by 100-MeV Ne^{6+}+He. The spectrum is displayed after background subtraction and transformation to the projectile rest frame. The observed Auger lines arise mainly from Li-like core-excited $1s2s^2$, $1s2s2p$, and $1s2p^2$ initial configurations. (See also Ref. [6]).

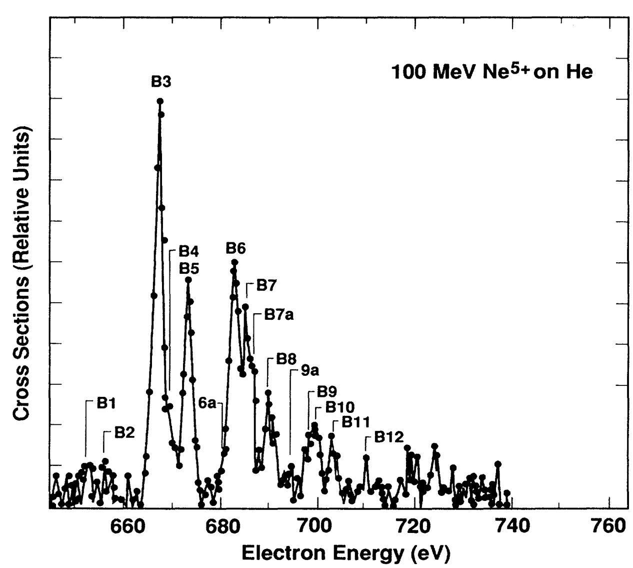

FIG. 2. High-resolution zero-degree electron spectrum produced by 100-MeV Ne^{5+}+He collisions. The spectrum is displayed after background subtraction and transformation to the projectile rest frame. The observed Auger lines arise mainly from Be-like core-excited $1s2s^22p$ and $1s2s2p^2$ initial configurations. (See also Ref. [6]).

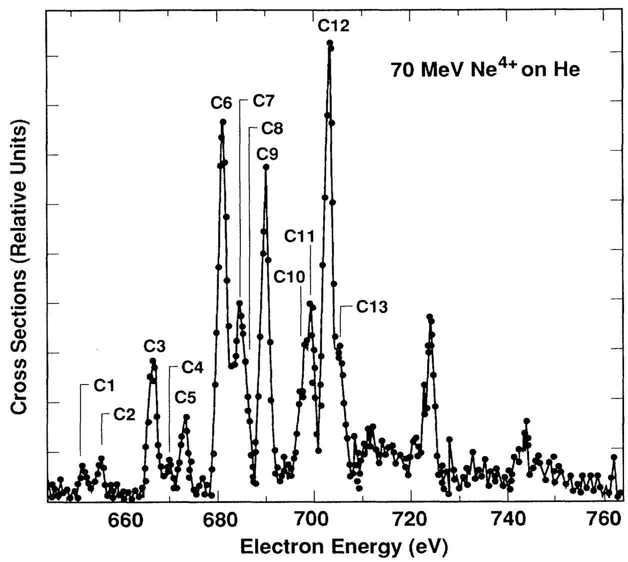

FIG. 3. High-resolution zero-degree electron spectrum produced by 70-MeV $Ne^{4+}+He$ collisions. The spectrum is displayed after background subtraction and transformation to the projectile rest frame. The observed Auger lines arise mainly from B-like core-excited $1s2s^22p^2$ and $1s2s2p^3$ initial configuration. (See also Ref. [6]).

taneous L-shell ionization or excitation processes have been observed as well.

In this work, the previous line assignment [6] for the measured Ne K Auger electron spectra has been substantially improved on the basis of new Auger energy, Auger rate, and branching ratio calculations including relativistic effects. In particular, K Auger states in Be-, and B-like Ne as they are produced in 100-MeV $Ne^{5+}+He$ and 70-MeV $Ne^{4+}+He$ have been carefully analyzed and the original line assignment is partially revised on the grounds of a very thorough study of the relativistic many-body problem for four- and five-electron systems. In addition, reliable Auger line intensity ratios for Be- and B-like states have been extracted. The line identification of the measured zero-degree electron spectra following 100-MeV $Ne^{6+}+He$, $Ne^{5+}+He$, and 70-MeV $Ne^{4+}+He$ is discussed in detail in the next section.

V. LINE ASSIGNMENT OF Ne K AUGER SPECTRA

A. Li-like states

The variation of the observed Auger electron spectra with incident projectile charge state is illustrated in Figs. 1–3. These figures clearly demonstrate the uniqueness of the method, since only a few individual Auger states are selectively excited in each spectrum. The discrete line structures in Fig. 1 are assigned as Auger transitions associated with electrons emitted mainly from Ne^{7+} single K-vacancy states. The detailed line identification is collected in Table VII together with theoretical results for comparison. As indicated in this table, the lowest feature $A1$ originates from the $(1s2s^2)^2S \rightarrow (1s^2\epsilon s)^2S$ transition. Our theoretical prediction of 652.66 coincides with the experimental value of 652.7 ± 0.1 eV and confirms our line identification. Recently, Kádár *et al.* [47] have reported an Auger energy of 652.47 for this transition, which deviates by 0.23 eV from the projectile Auger measurement. In our case, the 100-MeV $Ne^{6+}+He$ collision process forms Li-like $(1s2s^2)^2S$ states by direct single K-shell ionization. The next-higher peak, labeled $A2$ at 657.0 ± 0.1 eV is due to the metastable autoionizing $[1s(2s2p)^3P]^4P^\circ$ state, which is created most likely from

TABLE VII. Line assignment of the 100-MeV $Ne^{6+}+He$ Auger electron spectrum. The experimentally determined Auger transition energies are tabulated in comparison with theoretical predictions and other experimental values.

Peak label	System	Auger transition: Initial state	Auger transition: Final state	Auger transition energy (eV): Experiment: This work	Experiment: Other groups	Theory: This work	Theory: Other groups
$A1$	Li-like	$(1s2s^2)^2S$	$(1s^2)^1S$	652.7 ± 0.1	652.47^d 652 ± 1^b	652.66^a	
$A2$	Li-like	$[1s(2s2p)^3P]^4P^\circ$	$(1s^2)^1S$	657.0 ± 0.1	656.59^d 656 ± 1^b	657.03^a	
$A3$	Li-like	$[1s(2s2p)^3P]^2P^\circ$	$(1s^2)^1S$	669.0 ± 0.1	668.75^d 669 ± 1^b	669.12^a	
$A4$	Li-like	$(1s2p^2)^4P$	$(1s^2)^1S$	674.0 ± 0.1	674.05^d 674 ± 1^b	674.11^a	
$A5$	Be-like	$(1s2s2p^2)^3D$	$(1s^22p)^2P^\circ$	684.0 ± 0.4		683.99^c	684.4^b
						685.28^d	
$A6$	Be-like	$(1s2s2p^2)^3_bP$	$(1s^22p)^2P^\circ$	684.0 ± 0.4		684.28^c	
						684.57^d	
	Be-like	$(1s2s2p^2)^3D$	$(1s^22s)^2S$	700.0 ± 0.4		700.24^c	700.3^b
						701.42^d	
	Be-like	$(1s2s2p^2)^3_bP$	$(1s^22s)^2S$	700.0 ± 0.4		700.31^c	
						700.71^d	

[a]Saddle-point method including relativistic corrections, this work.
[b]Schumann *et al.* (Refs. [56,57]).
[c]$1/Z$ expansion (Refs. [17] and [24]).
[d]Kádár *et al.* (Ref. [47]).

the long-lived Ne VII $(1s^2 2s2p)^3P^\circ$ incoming beam component via single K-shell ionization. Moreover, the Auger line $A3$, centered at 669.0±0.1 eV, arises from the $[1s(2s2p)^3P]^2P^\circ$ state and is probably created by direct K-shell ionization from Ne VII $(1s^2 2s2p)^3P^\circ$. Recently, Zouros *et al.* [48] has suggested an alternative excitation process of $(1s2s2p)$ doublet and quartet states from ground-state ion beams by simultaneous inner-shell excitation or ionization and electron-electron excitation. However, the $[1s(2s2p)^1P]^2P^\circ$ states, which could be populated by this mechanism via K-shell ionization in conjunction with charge exchange, are not present in Fig. 1. Another prominent line, $A4$, centered at 674.0±0.1 eV is assigned as originating from $(1s2p^2)^4P$. This identification is supported by our theoretical transition energy of 674.11 eV. Finally, the peaks labeled $A5$ and $A6$ are due to Be-like $1s2s2p^2$ initial configurations. Since the metastable Ne VII $(1s^2 2s2p)^3P^\circ$ beam component already has one $2p$ electron, those $1s2s2p^2$ configurations may come from K-shell $1s \rightarrow 2p$ excitation of $(1s^2 2s2p)^3P^\circ$ projectile ions. The experimental and theoretical results summarized in Table VII clearly demonstrate that the projectile K Auger energies coincide within experimental uncertainties with our relativistic predictions. This, in turn, provides further evidence for the tremendous accuracy of the saddle-point variational

TABLE VIII. Line assignment of the 100-MeV Ne^{5+} + He Auger electron spectrum. The experimentally determined Auger transition energies are tabulated in comparison with theoretical predictions and other experimental values.

Peak label	System	Auger transition: Initial state	Auger transition: Final state	Auger transition energy (eV) Experiment: This work	Experiment: Other groups	Theory: This work	Theory: Other groups
$B1$	Li-like	$(1s2s^2)^1S$	$(1s^2)^1S$	652.7±0.2	652.47[e] 652±1[d]	652.66[a]	
$B2$	Li-like	$[1s(2s2p)^3P]^4P^\circ$	$(1s^2)^1S$	657.0±0.2	656.59[e] 656±1[d]	657.03[a]	
$B3$	Be-like	$(1s2s^2 2p)^3P^\circ$	$(1s^2 2p)^2P^\circ$	667.3±0.2	666.88[e] 665±1[d]	666.95[b] 667.83[c] 667.27[a]	667.8[d]
$B4$	Be-like	$(1s2s2p^2)^5P$	$(1s^2 2p)^2P^\circ$	670.3±0.2	669.86[e] 669±1[d]	670.50[b] 670.13[c] 670.12[f]	669.9[d]
$B5$	Be-like	$(1s2s^2 2p)^1P^\circ$	$(1s^2 2p)^2P^\circ$	673.4±0.1	673.62[e] 676±1[d]	673.26[b] 674.17[c]	674.5[d]
$B6a$	B-like	$(1s2s^2 2p^2)^4P$	$(1s^2 2p^2)^3P$	687.7±0.4	681.87[e]	681.82[b] 682.79[c]	
$B6$	Be-like	$(1s2s^2 2p)^3P^\circ$	$(1s^2 2s)^2S$	683.2±0.1	683±1[d] 683.05[e]	683.295[a] 682.97[b]	683.8[d]
$B7$	Be-like	$(1s2s2p^2)^3P$	$(1s^2 2p)^2P^\circ$	684±0.2		684.28[b] 684.57[c]	
$B7a$	Be-like	$(1s2s2p^2)^5P$	$(1s^2 2s)^2S$	686.3±0.4	687±1[d]	686.53[b] 686.31[c] 686.14[f]	
$B8$	B-like	$(1s2s^2 2p^2)^2P$	$(1s^2 2p^2)^3P$	690.4±0.4	690.06[e]	690.33[b] 691.19[c]	
$B9a$	Be-like	$(1s2s2p^2)^1D$	$(1s^2 2p)^2P^\circ$	694.0±0.4		693.18[b] 694.71[c]	
$B9$	B-like	$[1s2s(^3S)2p^3]^4S$	$(1s^2 2p^2)^3P$	694.0±0.4		693.18[b] 694.71[c]	
$B10$	Be-like	$(1s2s2p^2)^3D$	$(1s^2 2s)^2S$			700.24[b] 701.42[c]	
	B-like	$(1s2s^2 2p)^2P$	$(1s^2 2s2p)^1P^\circ$	699.8±0.4		699.67[b] 699.21[c]	
$B11$	B-like	$(1s2s^2 2p^2)^4P$	$(1s^2 2s2p)^3P^\circ$	703.7±0.4	704.60[e]	703.96[b] 705.06[c]	
$B12$	Be-like	$(1s2s2p^2)^1D$	$(1s^2 2s)^2S$	710.0±0.4		709.21[b] 710.84[c]	

[a]Saddle-point method including relativistic corrections, this paper.
[b]$1/Z$ expansion, Refs. [17,24] and this paper.
[c]Multiconfiguration Dirac-Fock calculations, this paper.
[d]Schumann *et al.* (Ref. [56]).
[e]Kádár *et al.* (Ref. [47]).
[f]Chung (Ref. [21], Phys. Rev. A **40**, 4203 (1989)).

method for Li-like states along the isoelectronic sequence.

B. Be-like states

The majority of the Auger lines displayed in Fig. 2 originate from Be-like initial configurations, namely, $1s2s^22p$ and $1s2s2p^2$. This energy region, however, also incorporates some weaker lines owing to Li- and B-like states, as can be clearly seen from Table VIII. For example, on the low-energy side of the 100-MeV $Ne^{5+}+He$ spectrum, we have assigned two individual lines, $B1$ and $B2$, as arising from Li-like $(1s2s^2)^2S$ and $(1s2s2p)^4P^\circ$ initial states. These levels may be formed by simultaneous K- and L-shell ionization in a single-collision event. However, from Fig. 2 and Table VI it is evident that the most probable excitation process leads to the Ne VII $(1s2s^22p)^3P^\circ$ and $^1P^\circ$ excited states via a single $1s$ ionization process. In order to make an unambiguous identification of these triplet and singlet states, we have performed extensive relativistic calculations including electron correlation. Based on predicted Auger line positions and partial rates, we have been able to make a complete line assignment of the Be-like K Auger structures. In fact, the strongest line observed, $B3$, results exclusively from the decay of $(1s2s^22p)^3P^\circ$. For this line, the calculated Auger transition energy of 667.27 eV perfectly agrees with the experimental value of 667.3 ± 0.1 eV. The relatively weak feature $B4$ is identified as coming from the metastable autoionizing $(1s2s2p^2)^5P$ term, which can decay relativistically through the $(1s^22p)^2P^\circ$ channel. We have also performed a careful theoretical study of the Be-like $(1s2s^22p)^1P^\circ$ state in Ne VII which can decay to the $1s^22p\epsilon s$ or ϵd and $1s^22s\epsilon p$ continua. Owing to accidental cancellation effects of the Auger transition matrix elements, the $(1s2s^22p)^1P^\circ$ resonance has only one principle Auger decay channel, namely $1s^22p\epsilon s$ leading to a nearly 100% population of the Ne VIII $(1s^22p)$ singly excited state [27]. This type of symmetry-favored Auger decay was first experimentally verified by Bruch *et al.* [2,3]. Consequently, peak $B5$ can be uniquely assigned as

TABLE IX. Line assignment of the 70-MeV $Ne^{4+}+He$ Auger electron spectrum. The experimentally determined Auger transition energies are tabulated in comparison with theoretical predictions and other experimental values.

Peak label	System	Auger transition: Initial state	Auger transition: Final state	Auger transition energy (eV) Experiment: This work	Experiment: Other groups	Theory: This work	Theory: Other groups
$C1$	Li-like	$(1s2s^2)^2S$	$(1s^2)^1S$	652.7 ± 0.2	652 ± 1[d]	652.66[a]	
					652.47[e]		
$C2$	Li-like	$[1s(2s2p)^3P]^4P^\circ$	$(1s^2)^1S$	657.0 ± 0.2	656 ± 1[d]	657.03[a]	
					656.69[e]		
$C3$	Be-like	$(1s2s^22p)^3P^\circ$	$(1s^22p)^2P^\circ$	667.2 ± 0.2	665 ± 1[d]	667.27[a]	667.8[d]
					666.88[e]	666.95[b]	
$C4$	Be-like	$(1s2s2p^2)^5P$	$(1s^22p)^2P^\circ$	670.3 ± 0.2	669.1 ± 1[d]	670.50[b]	669.9[d]
					669.86[e]		
$C5$	Be-like	$(1s2s^22p)^1P^\circ$	$(1s^22p)^2P^\circ$	673.8 ± 0.2	676 ± 1[d]	673.26[b]	674.5[d]
					673.62[e]		
$C6$	B-like	$(1s2s^22p^2)^4P$	$(1s^22p^2)^3P$	681.7 ± 0.1	681.87[e]	681.82[b]	
						682.79[c]	
$C7$	Be-like	$(1s2s^22p)^3P^\circ$	$(1s^22s)^2P^\circ$	683.2 ± 0.4	683.05[e]	683.295[a]	
	B-like	$(1s2s2p^3)^6S$	$(1s^22p^2)^3P$			682.97[b]	
						683.97[c]	
						683.42[c]	
$C8$	Be-like	$(1s2s2p^2)^5P$	$(1s^22s)^2S$	686.3 ± 0.4	687 ± 1[d]	686.53[b]	
					685.75[e]	686.31[c]	
$C9$	B-like	$[1s2s^22p^2(^3P)]^2P$	$(1s^22p^2)^3P$	690.4 ± 0.1	690.06[e]	690.33[b]	
						691.19[c]	
$C10$	B-like	$[1s2s(^3S)2p^3]^4S^\circ$	$(1s^22p^2)^3P$	699.3 ± 0.4		699.57[b]	
						699.43[c]	
$C11$	B-like	$[1s2s^22p^2(^3P)]^2P$	$(1s^22s2p)^1P^\circ$	699.8 ± 0.4		699.67[b]	
						699.21[c]	
$C12$	B-like	$(1s2s^22p^2)^4P$	$(1s^22s2p)^3P$	703.7 ± 0.1	704.60[e]	703.96[b]	
						705.06[c]	
$C13$	B-like	$(1s2s2p^3)^6S^\circ$	$(1s^22s2p)^3P^\circ$	706.2 ± 0.2		706.67[b]	
						705.68[c]	

[a]Saddle-point method including relativistic corrections, this paper.
[b]$1/Z$ expansion (Refs. [17,24]) and this paper.
[c]Multiconfiguration Dirac-Fock calculations, this paper.
[d]Schumann *et al.* (Ref. [56]).
[e]Kádár *et al.* (Ref. [47]).

coming from the

$$(1s2s^22p)^1P^\circ \rightarrow (1s^22p\epsilon s \text{ or } \epsilon d)^1P^\circ$$

Auger transition. The observed line energy of 673.4±0.1 eV agrees well with the $1/Z$ expansion result of 673.26 eV. This S-matrix approach of Safranova and co-workers [17] includes some electron-electron correlation effects and relativistic corrections. The next major peak, $B6$, originates from the

$$(1s2s^22p)^3P^\circ \rightarrow (1s^22s\epsilon p)^3P^\circ$$

Auger channel. In this case, the predicted saddle-point energy is 683.295 eV, which lies very close to the experimental value of 683.2±0.1 eV. A theoretical study of the $1s^22p$:$1s^22s$ intensity ratio for the $(1s2s^22p)^3P^\circ$ state supports this line identification. Furthermore, line $B7a$ is assigned as coming from the metastable autoionizing $(1s2s2p^2)^5P$ state. In this work, special attention is also given to the $1s^22p$:$1s^22s$ branching ratio associated with the lowest ^5P term (see Tables X and XI). Further prominent lines refer to the Be-like $(1s2s2p^2)$ configuration. Thus, peak $B7$ can be attributed to the $(1s2s2p^2)^3P$ state and peaks $B9a$, $B10$, and $B12$ refer mainly to the $(1s2s2p^2)^1D$ and ^3D states. In addition, some B-like Auger transitions have been observed, i.e., peaks $B6a$, $B8$, $B9$, $B10$, and $B11$, which can be attributed to $1s2s^22p^2$ initial configurations. These states can be created by $1s \rightarrow 2p$ K-shell excitation.

C. B-like states

The experimental electron spectrum for 70-MeV Ne^{4+}+He exhibits a few selective peaks as indicated in Fig. 3 and Table IX. These lines are mainly due to single K-shell ionization of the incident projectile and correspond to B-like initial states. It should be pointed out that such a rather pure B-like Auger spectrum allows new line assignments and determination of accurate Auger transition energies and branching ratios. Along with some revised assignments and corrections to those given in Ref. [6], we have studied in addition the Auger intensity ratio of the $(1s2s^22p^2)^4P$ state (see Table X). A few weaker lines associated with Li- and Be-like singly core-excited states are also observed at slightly lower energies and correspond to simultaneous K-shell plus double L-shell or K-shell plus single L-shell ionization.

Several interesting features are seen in Fig. 3 and Table IX. The lowest, dominant peak, $C6$, at 681.7±0.1 eV is due to the B-like $(1s2s^22p^2)^4P$ term decaying to the $(1s^22p^2)^3P$ state in Ne^{6+}. A schematic diagram illustrating the Auger decay of the $(1s2s^22p^2)^4P$ state is shown in Fig. 4. The arrows refer to the different decay channels. Each channel is specified by a bound state of the residual Ne^{6+} ion and MCDF branching ratios are shown as well. It is apparent from Fig. 4 that two predominant decay modes exist for the $[1s2s^22p^2(^3P)]^4P$ state, leading to 45% population of the $(1s^22p^2)^3P$ state and a 55% excitation of the $(1s^22s2p)^3P^\circ$ final states. With the help of these branching ratios, peaks $C6$ and $C12$ can be unambiguously assigned as the $[1s2s^22p^2(^3P)]^4P$ state. Specifically, the experimental Auger line energies for the $(1s^22p^2)^3P$ and $(1s^22s2p)^3P^\circ$ channels are 681.7±0.1 and 703.7±0.1 eV, respectively. These values are in good agreement with the $1/Z$ energies of 681.82 and 703.96 eV. We also note that the observed peak energy difference of 22.0 eV agrees reasonably well with 22.139

TABLE X. Comparison of experimental and theoretical K Auger intensity ratios resulting from Auger transitions of Ne VII $(1s2s^22p)^3P^\circ$, $(1s2s2p^2)^5P$, and Ne VI $(1s2s^22p^2)^4P$ terms.

				Experiment	Theory	
Ne^{q+}	Initial state	Decay channels	Intensity ratio	This work[a]	This work[b]	Other groups
6^+	$(1s2s^22p)^3P^\circ$	$(1s^22p)^2P^\circ$				0.93[c]
						2.08[d]
			$(1s^22p)^2P^\circ$:$(1s^22s)^2S$	1.65	1.90	1.69[e]
		$(1s^22s)^2S$				1.34[f]
						1.33[g]
6^+	$(1s2s2p^2)^5P$	$(1s^22p)^2P^\circ$				0.16[c]
			$(1s^22p)^2P^\circ$:$(1s^22s)^2S$	0.22	0.21	0.14[d]
		$(1s^22s)^2S$				0.09[e]
						0.17[f]
5^+	$[1s2s^22p^2(^3P)]^4P$	$(1s^22p^2)^3P$				
			$(1s^22p^2)^3P$:$(1s^22s2p)^3P^\circ$	0.83	0.82	0.685[f]
		$(1s^22s2p)^3P^\circ$				

[a]Zero-degree projectile Auger electron spectroscopy.
[b]Multiconfiguration Dirac-Fock model.
[c]$1/Z$ method (Ref. [24]) and this work.
[d]SUPERSTRUCTURE AUTO *LSJ*, Refs. [45,46].
[e]$Z_s = (Z-3)$ screening model, Ref. [24].
[f]Hartree-Fock-Slater model, Ref. [22].
[g]Hartree-Slater model, Ref. [23].

TABLE XI. Projectile and target K Auger line intensity ratio arising from the Ne VII $(1s2s^2 2p)^3P°$, $(1s2s2p^2)^5P$, and Ne VI $(1s2s2p2)^4P$ initial terms for different excitation processes.

Collision system	Initial state	Intensity ratio	Experimental results Projectile	Target
Ne^{5+} + He	Ne^{6+} $(1s2s^2 2p)^3P°$	$1s^2 2p/1s^2 2s$	1.65[a]	
Ar^{16+} + Ne				1.01[b]
Ne^{10+} + Ne				0.83[b]
Ar^{6+} + Ne				1.01[b]
Ne^{3+} + Ne				0.82[b]
Ne^{5+} + He	Ne^{6+} $(1s2s2p^2)^5P$	$1s^2 2p/1s^2 2s$	0.22[a]	
Ar^{16+} + Ne				0.43[b]
Ne^{10+} + Ne				0.35[b]
Ar^{6+} + Ne				0.36[b]
Ne^{3+} + Ne				0.22[b]
Ne^{4+} + He	Ne^{5+} $[1s2s^2 2p^2(^3P)]^4P$	$1s^2 2p^2(^3P)/1s^2 2s2p(^3P°)$	0.83	
Ne^{10+} + Ne				0.50[b]
Ar^{6+} + Ne				0.59[b]
Ne^{3+} + Ne				0.23[b]

[a]This work

[b]Kádár *et al.* (Ref. [47]).

eV, derived from optical measurements [49].

Two other quite pronounced Auger structures, labeled $C9$ and $C11$, have been observed in this study. They are attributed to the Ne^{5+} $[1s2s^2 2p^2(^3P)]^2P$ state, decaying predominantly to the $(1s^2 2p^2)^3P$ and $1s^2(2s2p)^1P°$ final ionic state (see Table IV). However, the peak around 699.8 eV may be perturbed by a close by transition, i.e.,

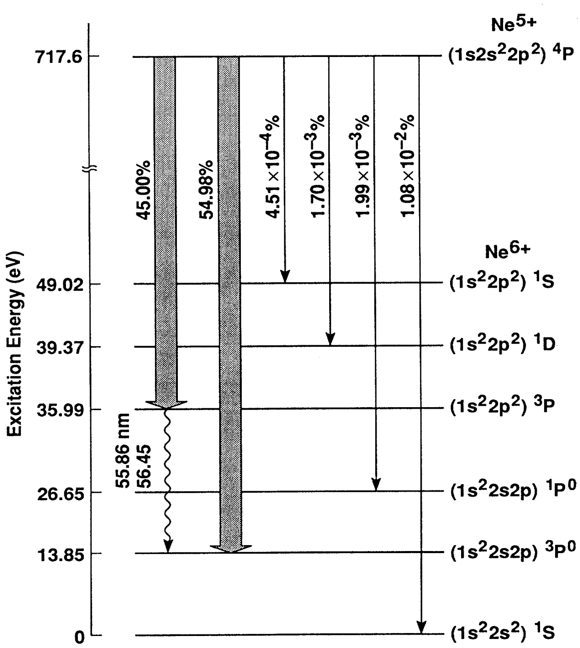

FIG. 4. Schematic K Auger decay diagram for the $(1s2s^2 2p^2)^4P$ state of Ne VI. The upper level refers to the K-vacancy state whereas the lower levels correspond to bound state of Ne VII. The arrows represent specific Auger transitions. The Auger branching ratios given have been calculated using the multiconfiguration Dirac-Fock model.

$$[1s2s(^3S)2p^3]^4S° \rightarrow [(1s^2 2p^2)^3P\epsilon p]^4S° ,$$

predicted at 699.43 eV by the MCDF model. The creation of this state requires a $1s \rightarrow 2p$ inner-shell excitation process.

In this study, we have also made an attempt to calculate Auger energies and rates of the metastable autoionizing $(1s2s2p^3)^6S$ term. According to Table IV, the most probable spin-induced decay channel leads to the $(1s^2 2s2p)^3P°$ final state. Therefore, peak $C13$ most probably arises from electron emission of the lowest sextet state in Ne VI. This identification is supported by our predicted MCDF energy of 705.68 eV. A second, important transition may populate the final $(1s^2 2p^2)^3P$ excited state (see Table IV). The MCDF energy for this channel is 683.42 eV, which is close to the Ne VII $(1s2s^2 2p)^3P° \rightarrow (1s^2 2s\epsilon p)^3P°$ line position. Hence, structure $C7$ may be an admixture of two lines originating from the $(1s2s^2 2p)^3P°$ and $(1s2s2p^3)^6S°$ initial states. Finally, peak $C8$ arises from Auger deexcitation of the Be-like $(1s2s2p^2)^5P$ level.

VI. AUGER LINE INTENSITY RATIOS

In this section we focus on Auger intensity ratios of the Ne^{6+} $(1s2s^2 2p)^3P°$, Ne^{6+} $(1s2s2p^2)^5P$ and Ne^{5+} $(1s2s^2 2p^2)^4P$ states, which are of fundamental importance to test different aspects of atomic many-body theories and relativistic interactions in multiply charged ions. To our knowledge, there does not seem to exist a careful experimental and theoretical comparison of such data for Be- and B-like systems. This information may also be crucial for the determination of absolute intensity and cross-section measurements following fast [1] and slow [50] ion-atom, ion-molecule, and ion-surface collisions [51].

In order to test K Auger rates calculated in various approximations, we have deduced line intensity ratios from high-resolution zero-degree projectile electron spectra. The procedure is shown in Figs. 5 and 6 for the Auger decay of the Ne VII $(1s2s^22p)^3P^\circ$ and Ne VI $(1s2s^22p^2)^4P$ states, respectively. As can be seen, Auger line profiles of the relevant peaks have been fitted by a Lorentzian curve, folded by a Gaussian-type spectrometer response function [2,3,6]. The experimental ratios thus obtained are summarized in Table X together with theoretical predictions. The most accurate way to calculate Auger rates is a theory including correlation and relativistic effects. Evidently the best agreement between experiment and theory is achieved by using the multiconfiguration Dirac-Fock model. For example, our MCDF calculation for the $(1s2s^22p^2)^4P$ term gives the result of 0.82 for the $(1s^22p^2)^3P$:$(1s^22s2p)^3P^\circ$ Auger line intensity ratio, whereas the experimental result is 0.83. If multiconfiguration effects are omitted, this ratio decreases to about 0.685 [Hartree-Fock-Slater (HFS) model]. In this connection, we further note that the $1s^22p$:$1s^22s$ ratio for $(1s2s^22p)^3P^\circ$ increases by approximately a factor of 1.4 when relativistic effects and configuration interaction are included in the atomic model. We can also learn from Tables VI and X that the Auger intensity ratios depend on the orbital and continuum wave functions used. For example, in the $Z_s = Z$-3 model, the continuum states $1s^22p\epsilon s$ or ϵd and $1s^22s\epsilon p$ are approximated by Coulomb wave functions and the radial wave function by hydrogenic functions. This model gives a very good result for the $(1s2s^22p)^3P^\circ$ state and, on the other hand, a poor result for the metastable autoionizing $(1s2s2p^2)^5P$ state.

It is also interesting to compare the measured "projectile" Auger intensity ratios with measured "target" Auger electron intensities [47] derived from complex Ne *K* Auger spectra. These target spectra have been induced by 5.5-MeV/u Ne^{3+}, Ne^{10+}, Ar^{6+}, and Ar^{16+} impact on

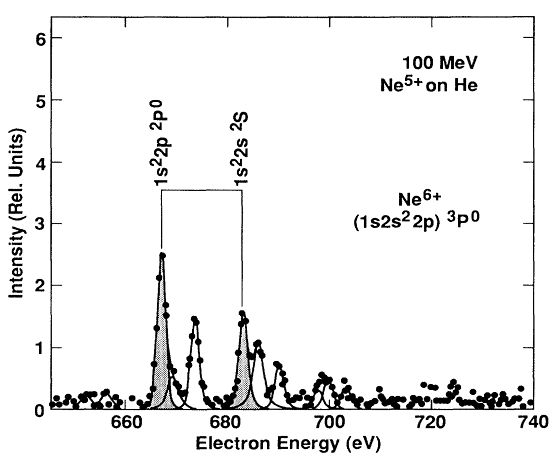

FIG. 5. Segment of a high-resolution projectile Auger electron spectrum indicating the two competing decay channels of the $(1s2s^22p)^3P^\circ$ state in Ne VII (lines labeled *B*3 and *B*6). The $1s^22p$:$1s^22s$ intensity ratio is 1.65 corresponding to a 62.3 and 37.7% population of the Ne VII $1s^22p$ and $1s^22s$ final states, respectively.

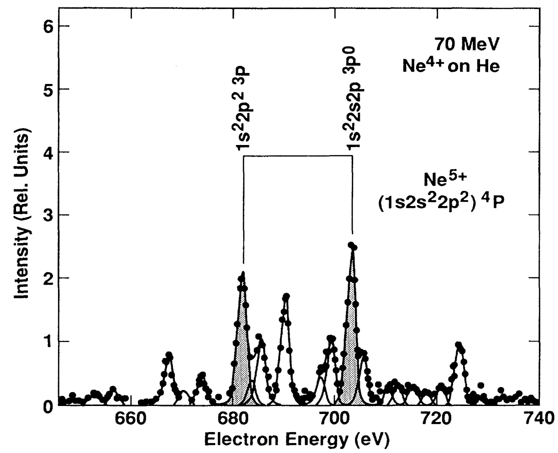

FIG. 6. Segment of a high-resolution projectile Auger electron spectrum indicating the two dominant decay channels of the $(1s2s^22p^2)^4P$ state in Ne VI. The $(1s^22p^2)^3P$:$(1s^22s2p)^3P$ intensity ratio is 0.83.

neon gas. In Table XI, our projectile intensity ratios are listed along with recent target data of Kádár *et al.* [47]. A striking result is the strong disagreement between target and projectile line intensity ratios. In particular, for the Coulomb autoionizing Ne VII $(1s2s^22p)^3P^\circ$ and Ne VI $(1s2s^22p^2)^4P$ states, the Ne target ratios are much smaller than our projectile data. On the other hand, for the metastable Ne VII $(1s2s2p^2)^5P$ state, Kádár and coworkers observed a larger intensity ratio when compared to our projectile Auger spectroscopy data. This disagreement between target and projectile data and the variation of Kádár and co-worker's ratios with different collision system (see Table XI) may be caused by principal difficulties with the target Auger spectroscopy method [52–55] such as overlapping Auger structures, cascade feeding mechanisms, and nonstatistical population of different fine-structure levels [55]. These complications generally do not occur in projectile Auger electron spectra following selective inner-shell ionization or excitation.

Finally, we note that Auger electron emission from foil-excited Ne ions (6–10 MeV) was measured by Schumann *et al.* [56,57]. The spectrum is separated into its isoelectronic parts by an Auger electron-ion coincidence technique which correlates the emitted electrons and emitted projectiles of well-defined charge states. However, owing to the complexity of the beam-foil excitation process and the limited statistics, those data are not very reliable for Be- and B-like states. Nevertheless, some of these data are included in our tabulations of energies and intensity ratios.

VII. SUMMARY AND CONCLUSION

In this paper we have provided a comprehensive study of Ne^{7+} (Li-like), Ne^{6+} (B-like), and Ne^{5+} (B-like) single-*K*-vacancy states. Such states can be excited by direct inner-shell excitation or by the dielectronic recombination process. Here we have investigated high-resolution projectile Auger electron spectra from core-excited fast neon ions produced by K-shell ionization or excitation following energetic Ne^{q+} $(q=6,5,4)+He$. For Be- and B-like states, the energy carried by an Auger electron depends on the decay channel and, hence, it is necessary to calculate not only reliable Auger transition energies but also Auger rates, branching ratios, and line intensity ratios. Therefore, we have studied characteristic properties of Auger matrix elements, Auger rates and intensity ratios, and Auger energy positions in terms of three different many-body approaches, namely, the saddle-point technique, the multiconfiguration Dirac-Fock model, and the $1/Z$ expansion method. Our theoretical results are compared with other results from the literature. In particular, our comparison on Auger rates and line intensity ratios clearly shows the importance of electron correlation and relativistic effects and the need for more extensive studies along isoelectronic series. At present, the best agreement between experimental and theoretical Auger intensity ratios has been obtained with MCDF model. If multiconfiguration effects are omitted, the experimental results cannot be reproduced. Specifically, we have shown that changes of the atomic model can change the Auger intensity ratio by as much as one order of magnitude. We have also predicted strong anomalies in emitted Auger intensities due to cancellations in Auger transition matrix elements. Similar phenomenon have been reported by Curtis and Ellis [58] for optical transitions. Still much can be learned from Auger intensity ratios in order to get a profound insight into the physics of complex wave functions associated with multiply charged highly excited states. Another important question to be solved by further studies is the role of relativistic effects on Auger rates along isoelectronic series.

ACKNOWLEDGMENTS

This work was performed in part under the auspices of the U.S. Department of Energy by Lawrence Livermore National Laboratory under Contract No W-7405-Eng-48. One of us (R.B.) is indebted to Dr. Ulyana I. Safronova from the U.S.S.R. Academy of Sciences, Institute of Spectroscopy, for communication of unpublished results and helpful comments. Furthermore, (R.B.) would like to thank the members of the "88" Cyclotron at the Lawrence Berkeley Laboratory and, in particular, Dr. Mike Prior, for their hospitality during his stay and the Lawrence Livermore National Laboratory for financial support. We gratefully acknowledge assistance from Stephan Fuelling at the Physics Department of the University of Nevada, Reno. R.B. would finally like to thank the members of the Max-Planck-Institut für Quantenoptik and, in particular, Professor H. Walther, for their hospitality and for financial support.

---

*Permanent address: Department of Physics, The University of North Carolina at Wilmington, Wilmington, NC 28403.

[1] N. Stolterfoht, Phys. Rep. **146**, 317 (1987).
[2] R. Bruch, N. Stolterfoht, S. Datz, P. D. Miller, P. L. Pepmiller, Y. Yamazaki, H. F. Krause, and J. K. Swenson, Phys. Rev. A **35**, 4114 (1987).
[3] R. Bruch, S. Datz, P. D. Miller, P. L. Pepmiller, H. F. Krause, J. K. Swenson, and N. Stolterfoht, Phys. Rev. A **36**, 394 (1987).
[4] D. Schneider, W. Zeitz, R. Kowalik, G. Schiwietz, T. Schneider, N. Stolterfoht, and U. Wille, Phys. Rev. A **34**, 169 (1986).
[5] D. Schneider, N. Stolterfoht, A. Schiwietz, T. Schneider, W. Zeitz, R. Bruch, and K. T. Chung, Nucl. Instrum. Methods B **24**, 173 (1987).
[6] A. Itoh, D. Schneider, T. Schneider, T. Y. M. Zouros, A. Nolte, A. Schiwietz, W. Zeitz, and N. Stolterfoht, Phys. Rev. A **31**, 684 (1985).
[7] M. H. Chen, At. Data Nucl. Data Tables **38**, 381 (1988).
[8] H. P. Kelly, in *Many-Body Perturbation Approaches to Calculation of Transition Probabilities, Atomic Inner-Shell Processes,* edited by Bernd Crasemann (Academic, New York, 1975), Vol. 1, p. 331.
[9] H. P. Kelly, Phys. Rev. A **11**, 556 (1975).
[10] R. L. Chase, H. P. Kelly, and H. S. Köhler, Phys. Rev. A **3**, 1550 (1971).
[11] D. R. Beck and C. Nicolaides, Int. J. Quantum Chem. Symp. **8**, 17 (1974).
[12] C. A. Nicolaides and Th. Mercouris, Phys. Rev. A **36**, 390 (1987).
[13] T. Mercouris and C. A. Nicolaides, Z. Phys. D **5**, 1 (1987).
[14] K. T. Chung and R. Bruch, Phys. Rev. A **28**, 1418 (1983).
[15] K. T. Chung, Phys. Rev. A **39**, 5483 (1989).
[16] R. Bruch, K. T. Chung, W. L. Luken, and J. C. Culberson, Phys. Rev. A **31**, 310 (1985).
[17] P. B. Ivanov and U. I. Safronova (unpublished).
[18] U. I. Safronova and L. A. Vainshtein, Nucl. Instrum. Methods B **9**, 359 (1985); L. A. Vainshtein and U. I. Safronova, At. Data Nucl. Data Tables **21**, 45 (1978); **25**, 311 (1980).
[19] M. H. Chen, Phys. Rev. A **31**, 1449 (1985).
[20] M. H. Chen, B. Crasemann, and H. Mark, Phys. Rev. A **24**, 1852 (1981).
[21] K. T. Chung, Phys. Scr. **42**, 530 (1990); Phys. Rev. A **40**, 4203 (1989).
[22] C. P. Bhalla, Electron Spectrosc. Relat. Phenom. **7**, 287 (1975).
[23] M. H. Chen and B. Crasemann, Phys. Rev. A **12**, 959 (1975).
[24] U. I. Safronova (private communication); J Dubau (unpublished).
[25] C. P. Bhalla, J. Phys. B **8**, 2792 (1975).
[26] D. Petrini, J. Phys. B **14**, 3839 (1981).
[27] C. D. Caldwell, M. G. Flemming, M. D. Krause, P. Van der Meulen, C. Pan, and A. Starace, Phys. Rev. A **41**, 542 (1990).
[28] R. Bruch and K. T. Chung, Comments At. Mol. Phys. **14**, 117 (1984).
[29] E. T. McGuire, Phys. Rev. Lett. **35**, 844 (1975).
[30] C. J. Keane, N. B. Ceglio, B. T. Mac Gowan, D. L. Matthews, D. G. Wilson, J. E. Trebs, and D. A. Whelan,

J. Phys. B **22**, 3343 (1989).
[31] H. C. Kapteyn, R. W. Lee, and R. W. Falcone, Phys. Rev. Lett. **57**, 2939 (1986).
[32] B. N. Chichkov and E. E. Fill, Opt. Commun. **74**, 202 (1989).
[33] B. N. Chichkov and E. E. Fill, Phys. Rev. A **42**, 599 (1990).
[34] Lawrence Berkeley Laboratory Advanced Light Source handbook No. PUB-643, Rev. 2 (unpublished); F. Schlachter (private communication).
[35] K. T. Chung, Phys. Rev. A **25**, 1596 (1982).
[36] M. H. Chen, Phys. Rev. A **15**, 2318 (1977).
[37] K. T. Chung, Phys. Rev. A **42**, 5726 (1990).
[38] K. T. Chung, Phys. Rev. A **29**, 682 (1984).
[39] W. Bambynek, B. Crasemann, R. W. Fink, H. U. Freund, H. Mark, C. D. Swift, R. E. Price, and P. V. Rao, Rev. Mod. Phys. **44**, 716 (1972).
[40] I. P. Grant, B. J. McKenzie, P. H. Norrington, D. F. Mayers, and N. C. Pyper, Comput. Phys. Commun. **21**, 207 (1980).
[41] M. H. Chen, Phys. Rev. A **31**, 1449 (1985).
[42] H. A. Bethe and E. E. Salpeter, *Quantum Mechanics of One- and Two-Electron Atoms* (Springer, Berlin, 1957).
[43] J. B. Mann and W. R. Johnson, Phys. Rev. A **4**, 41 (1971).
[44] B. J. McKenzie, I. P. Grant, and P. H. Norrington, Comput. Phys. Commun. **21**, 233 (1980).
[45] W. Eissner and H. Nussbaumer, J. Phys. B **2**, 1028 (1969).
[46] W. Eissner and H. Nussbaumer, Phys. Commun. **8**, 270 (1974).
[47] I. Kádár, S. Ricz, J. Végh, D. Varga, and D. Berényi, Phys. Rev. A **41**, 3518 (1990).
[48] T. J. M. Zouros, D. H. Lee, and P. Richard, in *The Physics of Electronic and Atomic Collisions,* proceedings of the Physics of Electronic and Atomic Collisions, AIP Conf. Proc. No. 205, edited by A. Dalgarno, R. S. Freund, P. M. Koch, M. S. Lubell, and T. B. Lucatorto (AIP, New York, 1989), p. 568.
[49] S. Bashkin and J. O. Stoner, *Atomic Energy Levels and Grotrian Diagrams* (North-Holland, Amsterdam, 1975), Vol. 1.
[50] D. Schneider, M. H. Chen, S. Chantrenne, R. Hutton, and M. H. Prior, Phys. Rev. A **40**, 4313 (1989).
[51] T. P. Briand, L. de Billy, P. Charles, S. Essabaa, P. Briand, R. Geller, T. P. Desclaux, S. Bliman and C. Ristori, Phys. Rev. Lett. **65**, 159 (1990).
[52] D. Schneider, C. Moore, and B. Johnson, J. Phys. B **9**, L153 (1976).
[53] D. L. Matthews, B. M. Johnson, J. J. Mackey, and C. F. Moore, Phys. Rev. Lett. **31**, 1331 (1973).
[54] N. Stolerfoht (unpublished).
[55] D. L. Matthews, R. T. Fortner, D. Schneider, and C. F. Moore, Phys. Rev. A **14**, 1561 (1976).
[56] S. Schumann, K. O. Groeneveld, A. Nolte, and B. Fricke, Z. Phys. A **289**, 245 (1979).
[57] S. Schumann, K. O. Groeneveld, Y. D. Levien, and B. Fricke, Phys. Lett. **60A**, 289 (1977).
[58] L. J. Curtis and D. A. Ellis, J. Phys. B **13**, L431 (1980).